Materials & Design 248 (2024) 113489

Contents lists available at ScienceDirect

Materials & Design

journal homepage: www.elsevier.com/locate/matdes

# Deciphering the mechanical strengthening mechanism: Soft metal doping in ceramic matrices-A case study of TiN-Ag films

Jing Luan [a,b,1], Fanlin Kong [a,1], Junhua Xu [a], Filipe Fernandes [b,c], Manuel Evaristo [b], Songtao Dong [a], Albano Cavaleiro [b], Hongbo Ju [a,b,d,*]

[a] Jiangsu University of Science and Technology, School of Materials Science and Engineering, Mengxi Road 2, Zhenjiang, Jiangsu Province 212003, China
[b] University of Coimbra, CEMMPRE, ARISE, Department of Mechanical Engineering, Rua Luís Reis Santos, 3030-788 Coimbra, Portugal
[c] CIDEM, ISEP – Polytechnic of Porto, Rua Dr. António Bernardino de Almeida, 4249-015 Porto, Portugal
[d] University of Ljubljana, Faculty of Mechanical Engineering, TINT – Laboratory for Tribology and Interface Nanotechnology, Aškerčeva 6, 1000 Ljubljana, Slovenia

ARTICLE INFO

*Keywords:*
Magnetron sputtering
Soft metal
Ceramic-based films
Epitaxy structure
Strengthening mechanism

ABSTRACT

Soft metals have been widely added into ceramic-based films for fully meeting the demanding requirements of green tribological applications. However, the resulting considerable increase of the mechanical strength by adding a soft metal below 5 at.%, which reversed the rule-of-mixture, was still not fully revealed. In this paper, a case study of TiN-Ag films was carried out to investigate the strengthening mechanism induced by adding soft metal in TiN-Ag composite/multilayered films deposited by magnetron sputtering. The results showed that dual-phases of fcc-TiN and fcc-Ag co-existed in the composite films with the Ag particles embedded in the matrix. In some areas of the Ag particles, with a size below 4 nm, epitaxial growth with the TiN template was detected, which obliged the lattice to be distorted and shrunken. Consequently, both hardness and elastic modulus were enhanced from 21 and 236 GPa, for the reference TiN film, to 26 and 323 GPa for the TiN-Ag composite film with 2.4 at.% Ag. The possibility of having the epitaxial growth of Ag within TiN were also confirmed by designing a TiN/Ag multilayered film with an Ag layer thickness of ~3 nm.

## 1. Introduction

Ceramic-based films, represented by nitride-based films, have become important star materials, for some critical mechanical components, to modify the surface properties due to their important properties of high hardness, excellent anti-corrosion and wear resistance [1–8]. Over the last two decades, extensive research has been conducted on these films, resulting in successful applications across various vital sectors such as aerospace, machining, and medical devices [9–15].

Over the recent years, there has been a notable trend in incorporating soft metals like gold (Au), silver (Ag), and copper (Cu) into hard ceramic-based films. These metals are utilized as additive elements with the aim of enhancing lubrication properties across a broad temperature spectrum, in addition to bolstering antibacterial capabilities. Such advancements are crucial for fully satisfying the stringent performance demands of critical aerospace and medical materials [16–25]. In the past few years, an extensive body of literature, close to 10,000 articles, has emerged from Web of Science focusing on ceramic-based systems containing soft metals, with particular emphasis from 2013 onwards. The consensus highlights that the introduction of a modest proportion of soft metal into the ceramic matrix, typically ranging from 1 to 3 atomic percent, consistently enhances the film's overall hardness. Nevertheless, it's noteworthy that a significant reduction in hardness occurs once the soft metal content surpasses 5 atomic percent [26–29]. Currently, the observed augmentation in hardness is commonly attributed to fine grain strengthening [26,27,30]. During the sputtering process, soft metal is integrated into the ceramic columnar grain boundaries in the form of nanocrystals, impeding the growth of ceramic grains [31–33]. Consequently, the mechanical properties of these films are bolstered through grain refinement strengthening. This enhancement is noteworthy, as the inherent soft mechanical strength of the soft metal may not adequately offset the effects of grain refinement strengthening, particularly given its relatively low content. Thus, the introduction of approximately 1 atomic percent of silver (Ag) into the TiN film through magnetron co-sputtering

* Corresponding author at: Jiangsu University of Science and Technology, School of Materials Science and Engineering, Mengxi Road 2, Zhenjiang, Jiangsu Province 212003, China.
*E-mail addresses:* hbju@just.edu.cn, hju@uc.pt (H. Ju).
[1] The co-first author.

https://doi.org/10.1016/j.matdes.2024.113489
Received 1 May 2024; Received in revised form 12 August 2024; Accepted 22 November 2024
Available online 23 November 2024

yields a substantial increase in hardness to around 29 GPa, contrasting with the reference TiN film's hardness of approximately 21 GPa, as demonstrated in our prior research [34]. However, this notable enhancement in mechanical properties cannot be solely attributed to the Hall-Petch principle, prompting further investigation into additional contributing factors. Upon thorough examination of relevant literature (Table 1), our experimental findings stand out as a unique case, showcasing the significant impact of low concentrations of soft metal on the mechanical strength improvement of ceramic-based films. The hardness increment, outlined in Table 1, attributed to soft metal addition surpasses that achieved through grain refinement strengthening. Furthermore, Table 1 also illustrates the residual stress within the films, indicating a modest influence of the soft metal due to its relatively limited presence. Consequently, the combined effect of grain refinement and residual stress on enhancing the mechanical properties of these films remains somewhat constrained.

In this paper, we present the design and deposition of TiN-Ag composite/multilayered films, showcasing a significant boost in mechanical strength. Our aim is to unveil the mechanism behind this enhanced strength induced by the addition of soft metal into a ceramic-based matrix. The choice of TiN as the matrix material was deliberate, given its prominence as one of the most representative ceramic-based films.

## 2. Experimental part

The deposition of TiN-Ag composite films was carried out through RF magnetron co-sputtering, utilizing separate high-purity targets of Ti (99.8 %) and Ag (99.8 %) with a 75 mm diameter, positioned 80 mm away from the substrate. Silicon wafers were employed as substrates for investigating both microstructure and mechanical properties, following a rigorous cleaning regimen involving ultrasonic immersion in alcohol for 15 min followed by acetone for an additional 15 min. Once the chamber's pressure was reduced to below $6.0 \times 10^{-4}$ Pa, a 100 nm thick pure Ti interlayer was first deposited onto the substrate. This step, conducted with an Ar flow rate of 10 sccm at a deposition pressure of 0.3 Pa, aimed to enhance film adhesion. Subsequently, nitrogen was introduced into the chamber via a gas mixture of $Ar/N_2$ at a ratio of 10/3 to deposit the composite film. The silver content in the film varied, with low content (~2.4 at.%) and higher content (~15.3, ~24.8 at.%), achieved by fixing the Ti target power at 200 W and adjusting the Ag target power to 30, 55, and 95 W, respectively. No bias or substrate heating was employed throughout the deposition process.

**Table 1**
The reported results of enhancing of mechanical strength by adding soft metal into ceramic-based films.

| Film system | Soft metal content (at.%) | Hardness (GPa) | Elastic modulus (GPa) | Grain size (nm) | Residual stress (GPa) |
|---|---|---|---|---|---|
| CrAlN-Ag [9] | 5 | 32, 28 (CrAlN) | 270, 250 (CrAlN) | 22, 25 (CrAlN) | / |
| TaN-Ag [17] | 3 | 40, 25 (TaN) | 360, 300 (TaN) | / | / |
| NbN-Ag [26] | 1.5 | 28, 17 (NbN) | 280, 200 (NbN) | 5, 38 (NbN) | / |
| $Mo_2N$-Ag [27] | 2.5 | 29, 24 (Mo2N) | / | / | / |
| HfN-Ag [28] | 0.3 (Ag/Hf) | 26, 20 (HfN) | 348, 322 (HfN) | 58, 65 (HfN) | 1.8, 1.9 (HfN) |
| TaN-Ag [30] | 1.2 | 31, 25 (TaN) | 338, 298 (TaN) | 6–9, 13 (TaN) | / |
| CrN-Cu [32] | 2–3 | 23, 13 (CrN) | 320, 160 (CrN) | / | / |
| TiAlVN-Cu [33] | 2.6 | 41, 32 (TiAlVN) | 501 | / | −5.7 |
| CrMoN-Ag [35,36] | 1.87 | 25, 22 (CrMoN) | 311, 206 (CrMoN) | / | / |
| VCN-Ag [37] | 0.72 | 29, 28 (VCN) | / | / | / |
| TiAlN-Ag [38] | 2.4 | 28, 25 (TiAlN) | / | / | / |
| MoVN-Cu [39,40] | 2.6 | 31, 15 (MoVN) | 450, 337 (MoVN) | / | / |
| NbCN-Cu [41] | 2.6 | 32, 27 (NbCN) | / | / | / |

The multilayered films were meticulously engineered with consistent thicknesses for both the Ti and Ag layers, approximately 10 nm and 3 nm, respectively. This precise design aimed to determine the critical size of Ag necessary for forming an epitaxial structure on the TiN template. The deposition process for these meticulously crafted multilayered films involved alternating the opening of shutters for the Ti target, operating at 200 W for 250 s, and the Ag target at 30 W for 4 s, respectively. All other deposition parameters remained consistent with those utilized for the composite films.

The elemental composition of the TiN-Ag composite films underwent analysis via Electron Probe Microanalysis (EPMA) using a CAMECA SX-50 instrument from France. To examine the crystal structure of the films, X-ray Diffraction (XRD) was conducted with a Shimadzu Shimazu-6000 instrument in Kyoto, Japan, utilizing Cu kα irradiation at a pass energy of 40 eV. The scanning range of 2θ spanned from 30 to 60°, with a step size of 1° during measurement. Observation of the cross-sectional microstructure of the composite/multilayered films was carried out using Transmission Electron Microscopy (TEM) with a JEOL JEM-2100F instrument from Japan, operating at a voltage of 200 kV. The TEM results presented in this paper were obtained from cross-sectional specimens prepared as follows: First, the as-deposited sample was glued with the film surface as the bonding surface, then cut into strips approximately 1.5 mm thick. These strips were polished down to about 50 μm and placed in an ion thinning instrument (Gatan 691, USA). The polished sample was thinned on both sides using an ion beam at an inclination angle of 8° until voids appeared. Finally, it was polished at 5° and 3° for 5 min, then removed and characterized by TEM. Hardness (H) and elastic modulus (E) measurements were performed via nano-indentation using equipment from Anton Paar in Switzerland (CPX + NHT2 + MST), applying a constant loading force of 3 mN and a holding time of 10 s. To ensure result accuracy, 15 measurements were taken in 2 different zones of the specimens.

## 3. Results and discussion

In Fig. 1(a), the TiN reference film is juxtaposed with TiN-Ag composite films featuring varying Ag content. Analysis of the X-ray

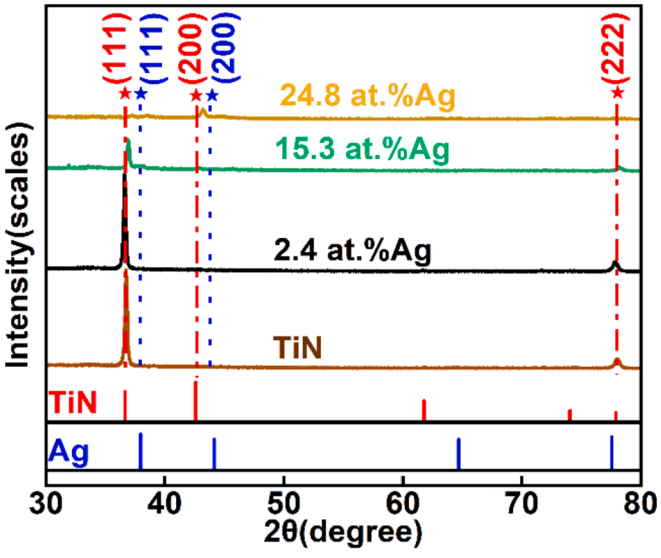


**Fig. 1.** XRD patterns of the TiN-Ag composite film with various Ag content.

diffraction (XRD) pattern of the TiN reference film reveals a singular face-centered cubic (fcc) structure, characterized by two distinct diffraction peaks corresponding to fcc-TiN (111) and (200), respectively (PDF #65-0715). Upon the addition of 2.4 at.% Ag into the TiN matrix, subtle shifts in the diffraction peaks towards lower angles are observed. This phenomenon is attributed to the contraction of the TiN lattice induced by Ag particles, which exhibit coherence with the TiN template (refer to the TEM section). The residual stress also attributes to the diffraction peak shifting (it decreased from +0.24 GPa for TiN to +0.20 GPa for TiN-Ag film at 2.4 at.% Ag). Furthermore, the coherent structure of Ag with TiN leads to an augmented intensity of (1 1 1) planes parallel to the surface, resulting in a slight enhancement of intensity. Notably, no discernible diffraction peaks corresponding to the Ag phase are detected due to its relatively low content. With a further increase in Ag content, the intensity of TiN diffraction peaks gradually diminishes, concomitant with the emergence of Ag diffraction peaks (PDF card #89-3722). The average grain size, computed using the Debye-Scherrer formula, corresponds to 64 nm, 59 nm, 34 nm, and 12 nm for Ag contents of 0 at.%, 2.4 at.%, 15.3 at.%, and 24.8 at.%, respectively. This trend suggests that Ag particles within the ceramic-based matrix effectively impede the coarsening of crystalline TiN, a phenomenon well-documented in the literature [42,43,44].

Transmission Electron Microscopy (TEM) was employed to delve deeper into the microstructure of the TiN-Ag film containing 2.4 at.% Ag (Fig. 2). The cross-sectional TEM image in Fig. 2(a) reveals a dense columnar morphology typical of the as-deposited film on the Ti interlayer. Additionally, it showcases darker nanoparticles uniformly dispersed throughout the matrix. These nanoparticles, previously identified as fcc-Ag phase based on prior research [30], segregate due to their extremely low solubility in the TiN lattice. The Selected Area Electron Diffraction (SAED) pattern shown in Fig. 2(b) displays two sets of diffraction rings, assigned to the fcc-TiN and fcc-Ag phases, respectively. Fig. 2(c) provides a High-Resolution TEM (HRTEM) image of the film, revealing a nanoparticle with a diameter of approximately 10 nm embedded within the matrix. The inverse Fast Fourier Transform (IFFT) and Fast Fourier Transform (FFT) images from region I in Fig. 2(c) are depicted in Fig. 2(d) and (e), respectively. A series of lattice fringes corresponding to the fcc-TiN (1 1 1) plane can be discerned based on a spacing of approximately 0.242 nm (PDF#65-0715). The FFT pattern in Fig. 2(e) also confirms a single fcc structure in region I. Region II, located within the nanoparticle, provides crystallographic information on the single fcc structure, with a lattice spacing of approximately 0.236 nm corresponding to fcc-Ag (1 1 1) (PDF card #89-3722), as shown in Fig. 2 (f), and (g). Consequently, the film consists of dual phases of fcc-TiN and

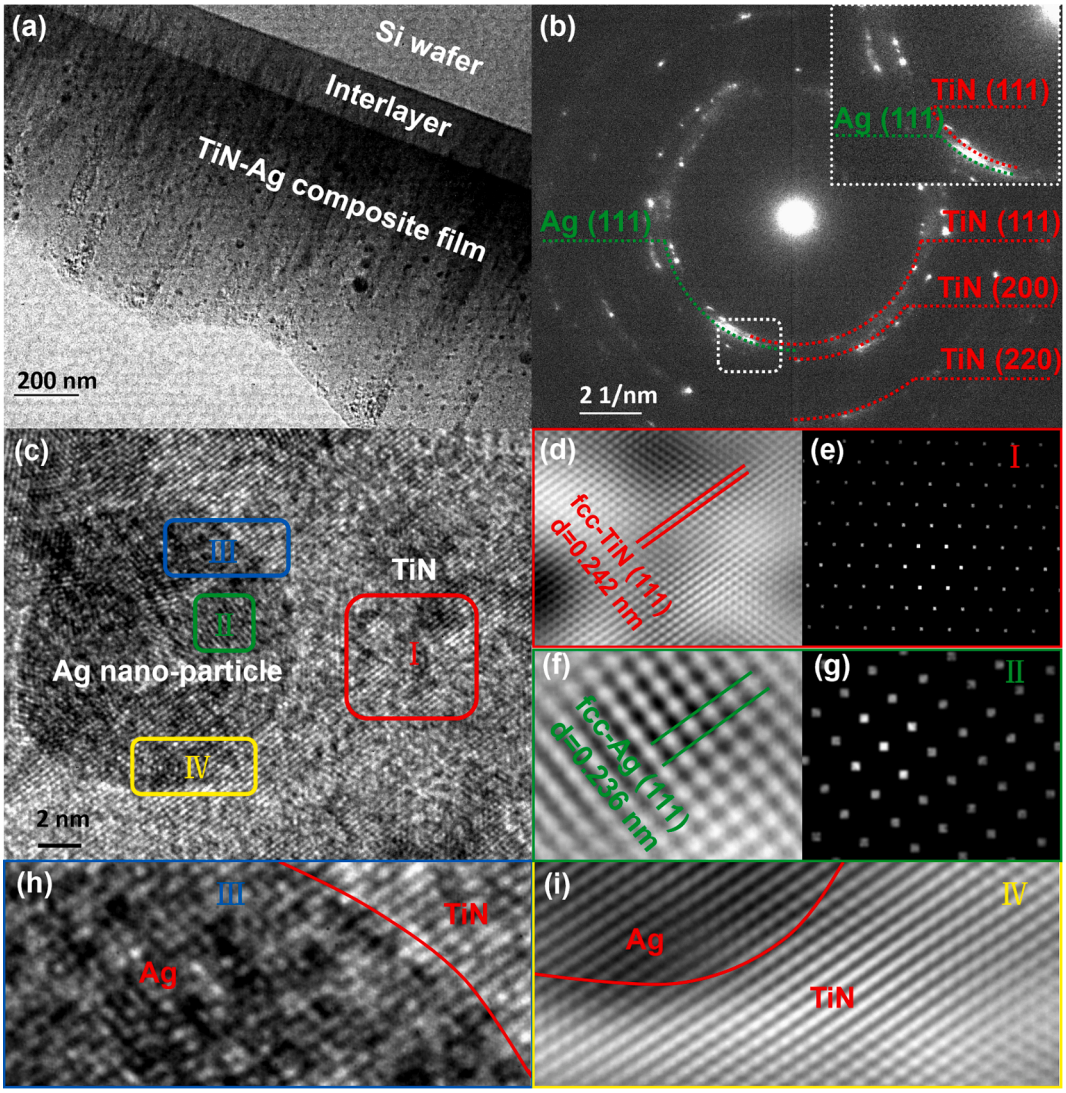


**Fig. 2.** TEM image of the cross-sectional TiN-Ag composite film with an Ag content of 2.4 at.% (a), SAED pattern from the as-deposited specimen (b), HRTEM image (c), IFFT image (d) from the region I in Fig. 3(c) and its FFT pattern (e), the IFFT image (f) and FFT pattern (g) from the inner of Ag nano-particle (region II in Fig. 3c), the IFFT images (h and i) from the TiN/Ag boundary in region III and IV in Fig. 3(c), respectively.

fcc-Ag, consistent with the results obtained from XRD, and SAED analyses. The interface characteristics from region III are depicted in Fig. 2 (h), where the TiN lattice fringes align nearly perpendicular to the tangent of the circular nanoparticle. The results reveal a coherent structure of fcc-Ag (1 1 1) with the fcc-TiN (1 1 1) phase, spanning approximately 3–4 nm in length. However, this coherence dissipates entirely beyond 4 nm from the template. Additionally, the High-Resolution TEM (HRTEM) image in Fig. 2(i), extracted from region IV in Fig. 2(c), portrays TiN (1 1 1) lattice fringes nearly parallel to the tangent of the nanoparticle, confirming an epitaxial structure of fcc-Ag on the fcc-TiN template. Notably, this structure seamlessly traverses the entire fcc-Ag phase.

The extension of the epitaxial structure of the Ag nanoparticles is markedly influenced by their size. A closer examination through cross-sectional TEM analysis of the multilayered film, comprising TiN layers approximately 10 nm thick and Ag layers around 3 nm thick, sheds light on the critical size of Ag for epitaxial growth (Fig. 3). In Fig. 3(a), the multilayered architecture is evident, with alternating layers of TiN (light) and Ag (black), and the measured thicknesses closely match the designed values. The SAED pattern of the multilayer film, depicted in Fig. 3(b), exhibits a set of diffraction rings corresponding to fcc-TiN (111), (200), and (220) from the inside to the outside, respectively. Notably, no other weak diffraction rings referencing the Ag phase appear in this pattern due to its complete epitaxial growth with the TiN template (it was confirmed by the HRTEM result). The HRTEM image in Fig. 3(c) reveals an epitaxial structure spanning several modulation layers. Notably, the thickness of the Ag layers (depicted in black) varies, ranging from thickest zones of about 4 nm to thinnest zones of just about 1.5 nm. This variability underscores the potential for Ag nanoparticles below 4 nm in size to undergo epitaxial growth following the TiN template. The limited wettability of soft Ag metal on the ceramic TiN matrix surface leads to the formation of a discontinuous Ag layer. Upon sputtering, Ag atoms tend to agglomerate on the TiN layer surface, resulting in dewetting. With the accumulation of more atoms, Ag agglomerates merge, forming an irregular layer that eventually achieves heterogeneous continuous thickness. Fig. 3(d) and (e) present FFT and IFFT patterns from the light layer (region I), respectively. The presence of a single fcc structure with a lattice fringe spacing of 0.242 nm (Fig. 3e) corresponds to the crystal plane of TiN (1 1 1) (PDF#65-0715). Fig. 3(f) and (g) show FFT and IFFT patterns from the epitaxy area (marked region II in Fig. 3c), respectively, revealing the interface zone. A single set of diffraction spots indexed to the fcc phase in the FFT pattern indicates a completely coherent structure, where the Ag lattice (dark area) epitaxially grows following the TiN template, as observed in the IFFT image.

Fig. 4 illustrates the hardness and elastic modulus of the TiN-Ag composite films, showcasing a significant enhancement in mechanical properties, including both hardness and elastic modulus, following the addition of a low content of Ag. Specifically, the measured hardness and elastic modulus of the multilayered film, featuring a 3 nm Ag layer thickness, are 30 GPa and 342 GPa, respectively. These values notably surpass those calculated using a rule-of-mixture (ROM, 16 GPa for Hardness, and 195 GPa for Elastic modulus).

Upon the observation of a reduction in average grain size resulting from the inclusion of 2.4 atomic percent (at.%) Ag, as evidenced by the XRD analysis, it becomes apparent that grain refinement strengthening alone cannot fully explain the notable increase in hardness. Instead, coherent strengthening emerges as a significant contributing factor, reminiscent of the well-established mechanism observed in Al-alloys during precipitation hardening. The substantial enhancement in hardness is attributed to the coherent growth of precipitates within the matrix, inducing distortion at the interface of the precipitates and the Al

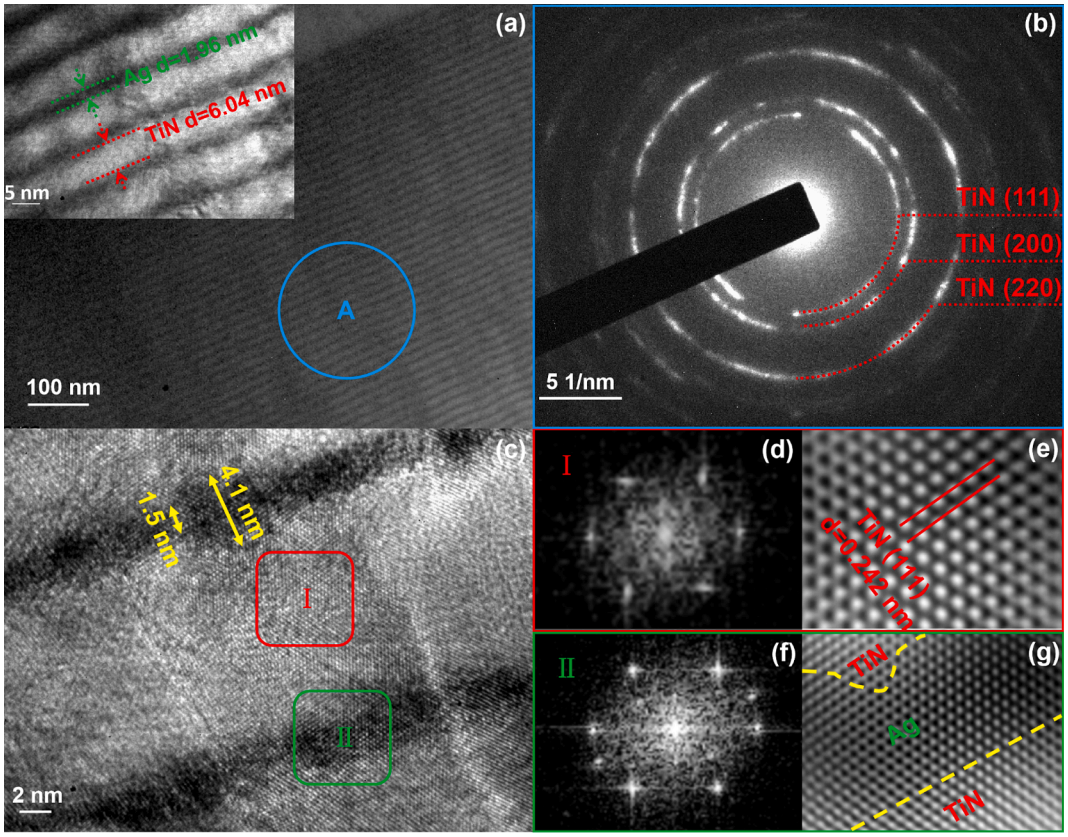


**Fig. 3.** TEM image of the cross-sectional multilayered film with a layer thickness of TiN ~ 10 nm, Ag ~ 3 nm (a), SAED pattern (b) of the multilayer film from the region A in Fig. 4(a), HRTEM image of its multilayer film (c), FFT (d), IFFT patterns (e) from the region I of Fig. 4(b), FFT (f), IFFT patterns (g) from the region II of Fig. 4(b).

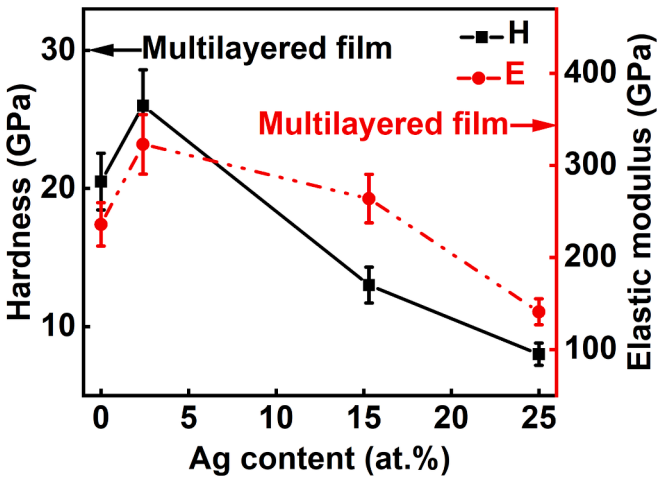


**Fig. 4.** Hardness and elastic modulus of the TiN-Ag composite films.

matrix (known as the GP – Guinier-Preston phenomenon) [45–47]. In regions where Ag nanoparticles exhibit coherence with the TiN matrix, spanning less than 4 nm, lattice distortion occurs as the lattice adjusts to accommodate the shorter lattice parameter of Ag. Consequently, the reduction in bond distance results in a slight increase in the elastic modulus of the TiN-Ag composite film containing 2.4 at.% Ag, compared to pure TiN. However, it's noteworthy that some Ag nanoparticles exceed the critical size for full coherency across the entire lattice, leading to the relaxation of this constraint and subsequently less distortion. This relaxation phenomenon is the primary reason why the maximum hardness of the composite film is lower than that of the multilayered film (as depicted in Fig. 4). Additionally, the significantly greater number of interfaces in the multilayered film compared to the composite film, also attributes to the higher hardness of the multilayered film. Similarly, the decrease in hardness with increasing Ag content can be attributed to the deposition of larger Ag particles, which impede the formation of a coherent structure spanning the entire Ag lattice. Consequently, both the hardness and elastic modulus of the composite film containing more than 2.4 at.% Ag align with those calculated using the ROM (20 GPa for Hardness, and 226 GPa for Elastic modulus).

## 4. Conclusion

In conclusion, our investigation has shed light on the principal mechanism driving the enhancement of mechanical properties when doping a ceramic-based hard matrix with a soft metal. Our analysis reveals that within TiN-Ag composite/multilayered films, certain regions containing Ag particles below 4 nm in size exhibit epitaxial growth with the TiN template. This phenomenon induces lattice distortion and contraction, thereby significantly bolstering both hardness and elastic modulus.

## CRediT authorship contribution statement

**Jing Luan:** Writing – review & editing, Writing – original draft, Methodology, Investigation. **Fanlin Kong:** Writing – review & editing, Writing – original draft, Methodology, Investigation. **Junhua Xu:** Supervision, Resources. **Filipe Fernandes:** Supervision, Data curation. **Manuel Evaristo:** Writing – review & editing. **Songtao Dong:** Investigation, Formal analysis. **Albano Cavaleiro:** Writing – review & editing, Investigation, Supervision, Resources. **Hongbo Ju:** Writing – review & editing, Writing – original draft, Validation, Supervision, Resources, Project administration, Methodology, Investigation, Funding acquisition, Formal analysis, Data curation, Conceptualization.

## Declaration of competing interest

The authors declare that they have no known competing financial interests or personal relationships that could have appeared to influence the work reported in this paper.

## Acknowledgements

Supported by the National Natural Science Foundation of China with the number of 52171071 and 51801081, national funds through FCT of Portugal – Fundação para a Ciência e a Tecnologia, under a scientific contract of 2021.04115.CEECIND, 2023.06224.CEECIND, and the projects of UIDB/00285/2020, and LA/0112/2020. The Slovenian Research Agency ARIS under the Research Core Funding Programme No. P2-0231 and the project MSCA-COFUND-5100-237/2023-9.

*Impact statement*

Unveiling Coherent Strengthening: The Key Mechanism behind Enhanced Mechanical Strength in Ceramic Matrices with Soft Metal Addition. This groundbreaking discovery marks a significant advancement, potentially the world's pioneering study.

## Data availability

Data will be made available on request.

## References

[1] A.V. Bondarev, D.G. Kvashnin, I.V. Shchetinin, D.V. Shtansky, Temperature dependent structural transfor- mation and friction behavior of nanocomposite VCN-(Ag) coatings, Mater. Des. 160 (2018) 964–973.
[2] H. Ju, R. Wang, N. Ding, L. Yu, J. Xu, F. Ahmed, B. Zuo, Y. Geng, Improvement on the oxidation resistance and tribological properties of molybdenum disulfide film by doping nitrogen, Mater. Des. 186 (2020) 108300.
[3] Y. Song, G. He, Y. Wang, Y. Chen, Tribological behavior of boron nitride nanoplatelet reinforced Ni3Al intermetallic matrix composite fabricated by selective laser melting, Mater. Des. 165 (2019) 107579.
[4] H. Ju, J. Guo, L. Yu, J. Xu, J. Luan, Enhancement of the mechanical and tribological properties of self-lubricant $Mo_2N$-Ag composite film by adding amorphous $SiN_x$, Ceram. Int. 50 (2024) 8463–8471.
[5] G. Vaitkunaite, C. Espejo, B. Thiebaut, A. Neville, A. Morina, Low friction tribofilm formation and distribution on an engine cylinder tested with MoDTCcontaining low viscosity engine lubricants, Tribol. Int. 171 (2022) 107551.
[6] H. Ju, N. Ding, J. Xu, L. Yu, I. Asempah, J. Xu, G. Yi, B. Ma, Crystal structure and the improvement of the mechanical and tribological properties of tungsten nitride films by addition of titanium, Surf. Coat. Technol. 345 (2018) 132–139.
[7] S. Komiyama, Y. Sutou, K. Oikawa, J. Koike, M. Wang, M. Sakurai, Wear and oxidation behavior of reactive sputtered δ-(Ti,Mo)N films deposited at different nitrogen gas flow rates, Tribol. Int. 87 (2015) 32–39.
[8] H. Ju, J. Luan, J. Xu, A. Cavaleiro, M. Evaristo, F. Fernandes, Nano-multilayered ZrN-Ag/Mo-S-N film design for stable anti-frictional performance at a wide range of temperatures, Friction, https://doi.org/10.1007/s40544-024-0943-y.
[9] P. Basnyat, B. Luster, Z. Kertzman, S. Stadler, P. Kohli, J.X. Samir Aouadi, S. R. Mishra, O.L. Eryilmaz, A. Erdemir, Mechanical and tribological properties of CrAlN-Ag self-lubricating films, Surf. Coat. Technol. 202 (2007) 1011–1016.
[10] H. Ju, J. Luan, Y. Wang, A. Bondarev, M. Evaristob, Y. Geng, J. Xu, A. Cavaleiro, F. Fernandes, Mutual promotion on the mechanical and tribological properties of the nacre-like self-lubricant film designed for demanding green tribological applications, Friction 13 (2025) 9440963.
[11] S. Klima, N. Jäger, H. Hruby, C. Mitterer, J.F. Keckes, M. Burghammer, R. Daniel, Structure-stress relation- ships in nanocrystalline multilayered $Al_{0.7}Cr_{0.3}N$/$Al_{0.9}Cr_{0.1}N$ coatings studied by cross-sectional X-ray nanodi- ffraction, Mater. Des. 170 (2019) 107702.
[12] H. Ju, K. Huang, J. Luan, Y. Geng, J. Yang, J. Xu, Evaluation under temperature cycling of the tribological properties of Ag-SiNx films for green tribological applications, Ceram. Int. 49 (2023) 30115–30124.
[13] C. Muratore, A. Voevodin, J. Hu, J. Zabinski, Multilayered YSZ-Ag-Mo/TiN adaptive tribological nanocomposite coatings, Tribol. Lett. 24 (2006) 201–206.
[14] C. Liu, Q. Bi, A. Matthews, Tribological and electrochemical performance of PVD TiN coatings on the femoral head of Ti-6Al-4V artificial hip joints, Surf. Coat. Technol. 163 (2003) 597–604.
[15] G. Małgorzata, A. Bukrym, E. Choińska, Effect of TiN coating on functional properties of implant titanium alloy, Solid State Phenom 147 (2009) 782–787.
[16] H. Ju, R. Zhou, S. Liu, L. Yu, J. Xu, Y. Geng, Enhancement of the tribological behavior of self-lubricating nanocomposite Mo2N/Cu films by adding the amorphous $SiN_x$, Surf. Coat. Technol. 423 (2021) 127565.

[17] P. Ren, X. Yang, S. Zhang, J. Qiu, Y. Li, L. Han, J. Zhang, M. Wen, Enhanced self-lubricating and antibacterial activity by building hard-yet-tough Ta-Ag-N films on Ti-6Al-4V, Surf. Coat. Technol. 403 (2020) 126423.
[18] H. Ju, R. Zhou, J. Luan, L. Yu, J. Xu, B. Zuo, J. Yang, Y. Geng, L. Zhao, F. Fernandes, Multilayer Mo2N-Ag/$SiN_x$ films for demanding applications: Morphology, structure and temperature-cycling tribological properties, Mater. Des. 223 (2022) 111128.
[19] Y. Zhao, X. Wang, J. Xiao, B. Yu, F. Li, Ti-Cu-N hard nanocomposite films prepared by pulse biased arc ion plating, Appl. Surf. Sci. 258 (2011) 370–376.
[20] Q. Zhang, Y. Zhou, G. Zhang, L. Zhang, Z. Xie, L. Zuo, H. Ju, Q. Fang, J. Liu, J. Yang, Nanocomposite Mo-Ag-N lubricating, wear resistant and hard coatings fabricated by magnetron sputtering, Mater. Sci. Eng. B 286 (2022) 116066.
[21] H. Ju, D. Yu, L. Yu, N. Ding, J. Xu, X. Zhang, Y. Zheng, L. Yang, X. He, The influence of Ag contents on the microstructure, mechanical and tribological properties of ZrN-Ag films, Vacuum 148 (2018) 54–61.
[22] J. Luan, F. Kong, M. Evaristo, F. Fernandes, Y. Zhou, A. Cavaleiro, H. Ju, Design and magnetron sputtering of nanomultilayered $W_2N$/Ag-$SiN_x$ films: Microstructural insights and optimized self-lubricant properties from room temperature to 500 °C, Ceramics Int., https://doi.org/10.1016/j.ceramint.2024.07.292.
[23] J. Luan, H. Lu, J. Xu, F. Fernandes, M. Evaristo, B. Ma, F. Xie, A. Cavaleiro, H. Ju, Exploring tribological characteristics of ZrN-MoSN composite films fabricated via RF magnetron sputtering: Insights from microstructure and performance analysis, Surf. Coat. Technol. 484 (2024) 130813.
[24] H. Mei, J. Ding, K. Yan, W. Peng, C. Zhao, Q. Luo, W. Gong, F. Ren, Q. Wang, Effects of V and Cu codoping on the tribological properties and oxidation behavior of AlTiN coatings, Ceram. Int. 48 (2022) 22276–22286.
[25] J. Xu, H. Ju, L. Yu, Microstructure, oxidation resistance, mechanical and tribological properties of MoeAleN films by reactive magnetron sputtering, Vacuum 103 (2014) 21–27.
[26] P. Ren, K. Zhang, X. He, S. Du, X. Yang, T. An, M. Wen, W. Zheng, Toughness enhancement and tribochemistry of the Nb-Ag-N films actuated by solute Ag, Acta Mater. 137 (2017) 1–11.
[27] W. Gulbiński, T. Suszko, Thin films of $Mo_2N$/Ag nanocomposite—the structure, mechanical and tribological properties, Surf. Coat. Technol. 201 (2006) 1469–1476.
[28] G. Wang, Y. Si, M. Wen, J. Qiu, S. Zhang, Q. Song, W. Wang, X. Yang, P. Ren, Microstructure, mechanical and tribological behaviors of hard-yet-tough Hf-Ag-N coating, J. Mater. Res. Technol. 22 (2023) 2030–2042.
[29] H. Ju, J. Xu, Microstructure and tribological properties of NbN-Ag composite films by reactive magnetron sputtering, Appl. Surf. Sci. 355 (2015) 878–883.
[30] H. Li, J. Li, J. Kong, J. Huang, Q. Wu, D. Xiong, Achieving high toughness and wear resistance for hard TaN-Ag films actuated by Ag, Int. J. Refract Metal Hard Mater. 111 (2023) 106076.
[31] H. Ju, N. Ding, J. Xu, L. Yu, Y. Geng, F. Ahmed, B. Zuo, L. Shao, The influence of crystal structure and the enhancement of mechanical and frictional properties of titanium nitride film by addition of ruthenium, Appl. Surf. Sci. 489 (2019) 247–254.
[32] J.W. Lee, Y. Kuo, Y.C. Chang, Microstructure and mechanical properties of pulsed DC magnetron sputtered nanocomposite Cr-Cu-N thin films, Surf. Coat. Technol. 201 (2006) 4078–4082.
[33] H. Mei, D. Geng, R. Wang, L. Cheng, J. Ding, Q. Luo, T. Zhang, Q. Wang, Effect of Cu doping on the microstructure and mechanical properties of AlTiVN-Cu nanocomposite coatings, Surf. Coat. Technol. 402 (2020) 126490.
[34] H. Ju, L. Yu, D. Yu, I. Asempah, J. Xu, Microstructure, mechanical and trobological properties of TiN-Ag films deposited by reactive magnetron sputtering, Vacuum 141 (2017) 82–88.
[35] F. Zhou, J. Qian, M. Zhang, Y. Wu, Q. Wang, Z. Zhou, Tribocorrosion properties of CrMoN/Ag coatings with various Ag contents in seawater, Surf. Coat. Technol. 473 (2023) 129993.
[36] L. Yeh-Liu, S. Hsu, P. Chen, J. Lee, J. Duh, Improvement of CrMoN/SiNx coatings on mechanical and high temperature Tribological properties through biomimetic laminated structure design, Surf. Coat. Technol. 393 (2020) 125754.
[37] D. Yu, L. Yu, I. Asempah, H. Ju, J. Xu, S. Koyama, Y. Gao, Microstructure, mechanical and tribological properties of VCN-Ag composite films by reactive magnetron sputtering, Surf. Coat. Technol. 399 (2020) 126167.
[38] M. Ren, H. Yu, L. Zhu, H. Li, H. Wang, Z. Xing, B. Xu, Microstructure, mechanical properties and tribological behaviors of TiAlN-Ag composite coatings by pulsed magnetron sputtering method, Surf. Coat. Technol. 436 (2022) 128286.
[39] J. Ding, H. Mei, Q. Li, Z. Zhao, Y. Shen, L. Cheng, R. Wang, W. Gong, Q. Wang, Microstructure, mechanical and tribological properties of Mo–V–Cu–N coatings prepared by HIPIMS technique, Ceram. Int. 48 (2022) 10704–10712.
[40] W. Wang, J. Pu, Z. Cai, S. Zheng, Y. Wei, Insights into friction properties and mechanism of self-lubricating MoVN–Ag films at high temperature, Vacuum 176 (2020) 109332.
[41] S. Bian, L. Yu, P. Jia, J. Xu, Study on microstructure, mechanical properties and corrosion resistance of NbCN-Cu composite films, Int. J. Refract Metal Hard Mater. 107 (2022) 105885.
[42] C. Tseng, J. Hsieh, S. Jang, Y. Chang, W. Wu, Microstructural analysis and mechanical properties of TaN-Ag nanocomposite thin films, Thin Solid Films 517 (2009) 4970–4974.
[43] K. Kitawaki, K. Kaneko, K. Inoke, J. Hernandez-Garrido, P. Midgley, H. Okuyama, M. Uda, Y. Sakka, Fabrication and characterization of TiN-Ag nano-dice, Micron 40 (2009) 308–312.
[44] H. Ju, L. Xu, J. Luan, Y. Geng, J. Xu, L. Yu, J. Yang, F. Fernandes, Enhancement on the hardness and oxidation resistance property of TiN/Ag composite films for high temperature applications by addition of Si, Vacuum 209 (2023) 111752.
[45] H. Miyoshi, H. Kimizuka, A. Ishii, S. Ogata, Temperature-dependent nucleation kinetics of Guinier-Preston zones in Al-Cu alloys: An atomistic kinetic Monte Carlo and classical nucleation theory approach, Acta Mater. 179 (2019) 262–272.
[46] G. Sha, R. Marceau, X. Gao, B. Muddle, S. Ringer, Nanostructure of aluminium alloy 2024: Segregation, clustering and precipitation processes, Acta Mater. 59 (2011) (2024) 1659–1670.
[47] C. Singh, D. Warner, Mechanisms of Guinier-Preston zone hardening in the athermal limit, Acta Mater. 58 (2010) 5797–5805.